Semiconductor Physics, Quantum Electronics & Optoelectronics, 2026. V. 29, No 2. P. 246-260.

Optoelectronics and optoelectronic devices

Thin composite films with a perfluoropolymer matrix deposited from the gas phase: properties and novel applications (Review)

K.P. Grytsenko[1*], O.L. Kukla[1], A.I. Biletskiy[1], H.S. Kashyna[2], Y.V. Kutafin[2], M. Prelipceanu[3], A. Grebinyk[4], E.V. Vashchilina[5]

[1]*V. Lashkaryov Institute of Semiconductor Physics of NASU, 41 Nauky Avenue, 03028 Kyiv, Ukraine*
[2]*Academy of Labor, Social Relations and Tourism, 3-A Kiltseva Road, 03187 Kyiv, Ukraine*
[3]*Stefan cel Mare University of Suceava, 13, Universitatii Street, Building D, Suceava, 720229, Romania*
[4]*Photo Injector Test Facility at German Electron Synchrotron (DESY), Platanenallee 6, D-15738 Zeuthen, Germany*
[5]*T. Shevchenko National University of Kyiv, 64/13 Volodymyrs'ka Str., 01601 Kyiv, Ukraine*
[*]*Corresponding author e-mail: d.grytsenko@gmail.com*

Abstract. The properties and applications of perfluoropolymer nanocomposite thin films deposited from the gas phase are summarized, and the development trends in this field are discussed in this review. The perfluoropolymer matrix protects metal nanoparticles from corrosion, imparts superhydrophobic properties to surfaces, extends the lifetime of medical implants, and improves the performance of functional layers in organic light-emitting diodes, among other applications. Dyes and metal nanoparticles incorporated into the PTFE matrix demonstrate unique properties, making these materials promising for optical and biomedical applications.

Keywords: perfluoropolymer, polytetrafluoroethylene, thin film, matrix, nanocomposite, dye.

https://doi.org/10.15407/spqeo29.02.246
PACS 78.40.Me, 81.05.Qk, 81.15.-z, 82.35.Np

Manuscript received 23.04.26; revised version received 03.06.26; accepted for publication 10.06.26; published online 23.06.26.

1. Introduction

Polymer-based nanocomposites (NCs) have recently garnered attention for their unique physicochemical properties, which make them highly suitable for applications in optics, sensing, and the life sciences. Initial research on these materials dates to the 1980s, originating as scientific inquiries [1, 2]. These films were evaluated as laser recording media [3, 4]. Various methods have been developed for the gas-phase deposition of metal-filled polymer films, including magnetron sputtering (MSp) of gold (Au) targets in C_2F_3Cl or C F_4/Ar mixtures, plasma polymerization of metal-organic compounds with perfluoromonomers, and physical vapor co-deposition (PVD) of metals and polymers. An overview of the earlier stages in the development of deposition technologies and the properties of various polymer thin films is presented in [4]. Each deposition technique presents specific advantages, making them suitable for thin films with tailored properties. Among them, perfluoropolymer (PFP) films filled with metal and dye nanoparticles (NPs) have demonstrated superior performance and are currently being tested for various high-tech industrial applications. This paper aims to present a detailed analysis of the multifunctional properties imparted by the perfluoropolymer matrix and summarize information on the fabrication, optical properties, and applications of nanocomposite thin films based on the PFP matrix.

2. PFP thin film filled with inorganic NPs

2.1. PTFE films filled with noble metal NPs

Electroconductive solid lubricant films formed using biased RF sputtering have been developed to combine the electrical conductivity of Au with the low surface energy of PTFE [5]. These films were fabricated as either multilayer structures (100 alternating layers) or NC films. The balance between electrical and surface properties was achieved by controlling the chemical composition and modulating the deposition power. In NC films with lower fluorine and carbon concentrations, the electrical resistivity was measured at 0.02 Ω·cm. By increasing the concentration of fluorine (up to 18 at.%) and carbon (up to 10 at.%), the surface free energy was reduced to 29 mN/m. The structural control was achieved through the RF power: under lower power (100 W target/18 W substrate), the films developed a multilayer structure with a period of 4 nm. This suppressed grain growth resulted in surface smoothness with a centerline average roughness of 0.3 to 0.5 nm. In low-load friction tests (10 mN), these multilayers exhibited friction coefficients of 0.05 in air.

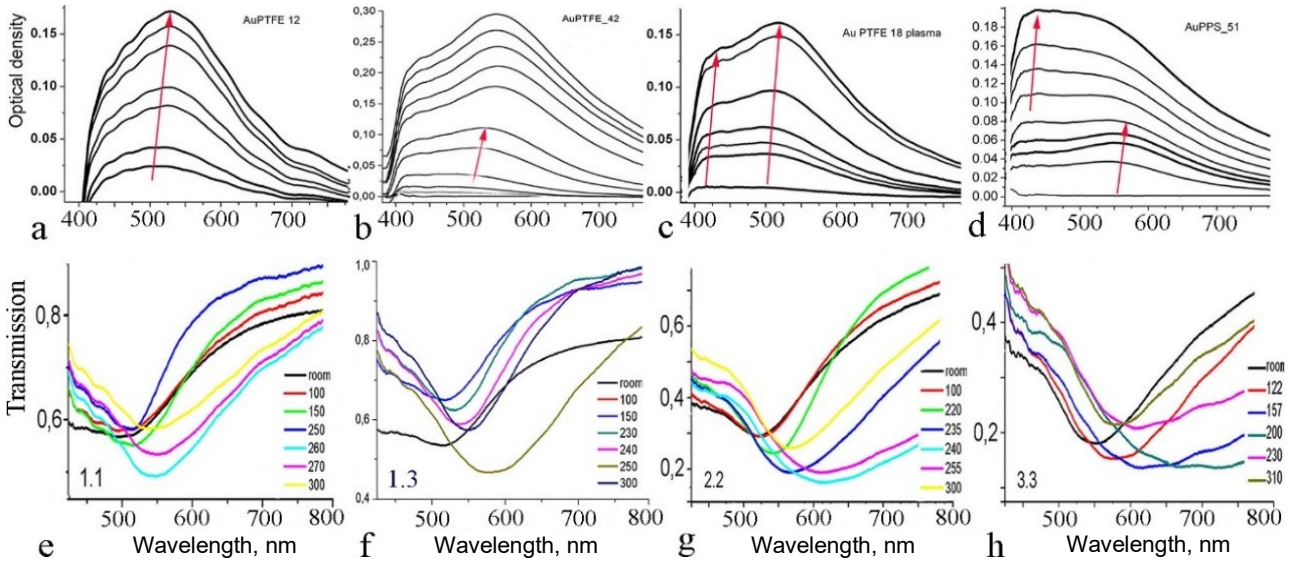

Fig. 1. Evolution of the optical spectra of Au + PTFE and Au + PPS films recorded during growth and subsequent heating. Au12 and Au42 were deposited *via* EAVD, while Au18 was deposited *via* PAEVD. The numbers in the bottom-left corner of the spectra correspond to the sample designations in Fig. 2. Figures are adapted from Ref. [4].

Films deposited at higher power (200 W target / 50 W substrate) exhibited a larger surface roughness of 7.0 to 9.2 nm due to formation of Au and PTFE NPs rather than uniform layers. While this roughness elevated the dry friction coefficient, these NPs provided the mechanical robustness to endure high-load tests (10 N). The wear durability of films deposited under higher power was superior under lubrication with distilled water, tap water, and polyalphaolefin. This allows the customization of films performance: lower power for precision low-load applications and higher power for boundary lubrication environments where wear durability is required [5].

NC films consisting of Ag NPs embedded in a Teflon AF matrix, co-deposited *via* PVD, were investigated in [6]. The electrical conductivity of these composites was measured *in situ* as a function of film thickness at various Ag concentrations. At low metal concentrations (< 30%), the films exhibited dielectric behavior with little dependence on thickness. However, at moderate to high silver content (30…80%), an increase in electrical conductivity was observed as the films grew thicker, eventually reaching a plateau. At silver content > 90%, fragmented NPs interconnected to achieve percolation, ultimately evolving into a metallic continuum with Teflon inclusions.

NP-filled PTFE films were earlier investigated in works [3, 4, 7–10] for optoelectronic applications. NPs within a PFP matrix were deposited using the developed electron-activated vacuum deposition (EAVD) and additional plasma-activated EAVD (PAEVD) methods. Other fluoropolymers, such as polychlorotrifluoroethylene (PClTFE) and Cytop, were utilized for film production. PTFE and poly(paraphenylene sulfide) (PPS) films were filled with Au NPs *via* EAVD co-deposition [7]. Film formation was studied *in situ* using optical spectroscopy. The scheme of the deposition system is presented in [4, 7]. Fig. 1 illustrates the evolution of the optical spectra for Au + PTFE and Au + PPS films grown both with EAVD and PAEVD, as well as during subsequent heating in air. Fig. 2 shows TEM images of as-deposited and AFM images of annealed Au + PTFE films. Fig. 1 shows that at the initial stage of film growth, small Au NPs with a plasmon band at 480 nm are formed. Subsequently, NP aggregation causes a red shift of the plasmon band to 520…550 nm, depending on the Au concentration. The diameter of these Au NPs ranges from 2 to 8 nm. PAEVD results in the formation of smaller but aggregated Au NPs. When PPS is used as a matrix, the EAVD growth kinetics reveals a two-step mechanism. At the onset of film growth, Au NPs with a plasmon band at 600 nm are formed. With increasing film thickness, the intensity of the band at 420 nm grows more rapidly, becoming the dominant peak in the final film. PAEVD leads to the formation of Au aggregates confined within the PPS matrix, exhibiting a plasmon band at 620 nm.

From Fig. 2, one can see that the NP size increases at higher Au concentrations. During heating up to 300°C, the evolution of the plasmon band wavelength and shape is non-linear and depends on both Au concentration and annealing temperature. This complexity stems from the distinct thermal behaviors of the properties of two materials within the composite. Fig. 3 shows the morphology of the laser-treated Al- Au- and dye-filled PTFE films. One can see that Al oxide NPs increased in size and the interparticle distance decreased, while the PTFE matrix was partially eliminated under the electron beam.

Treatment of Au + PTFE films with a focused excimer laser beam enables the production of micro-domains with controlled Au NPs growth [9]. High laser power densities resulted in ablation of the deposited films, whereas decreasing the power density allowed to produce metal spots.

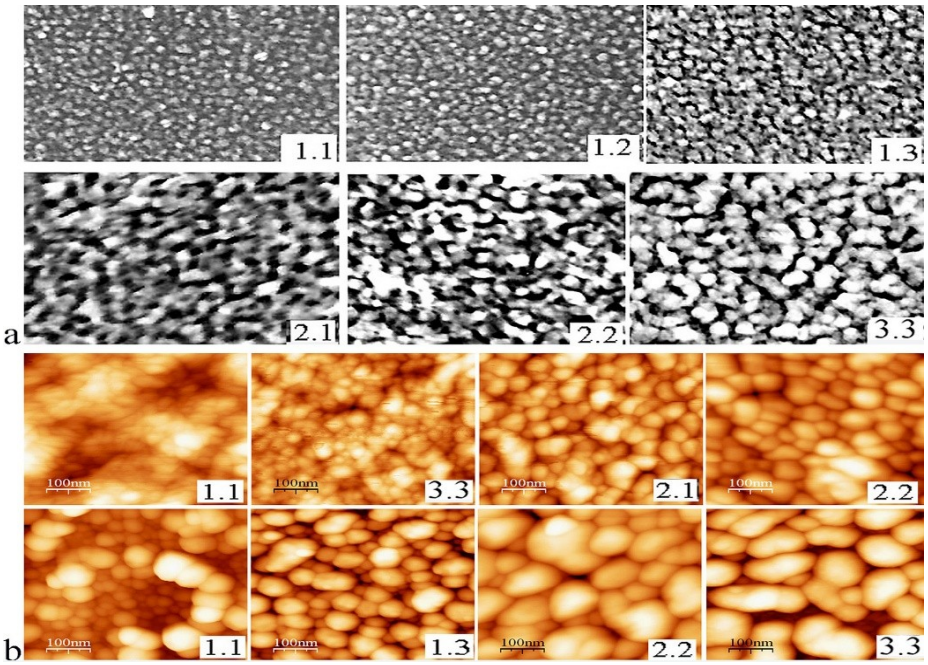

Fig. 2. a) TEM (magnification 100 000) of as-deposited Au + PTFE films; b) AFM of annealed Au + PTFE films: 1.1 – heated to 150 °C, 3.3 – heated to 150 °C, 2.1 – heated to 220 °C, 2.2 – to 20 °C; bottom row 1.1, 1.3, 2.2, 3.3 – all heated to 300 °C. Adapted from Ref. [8].

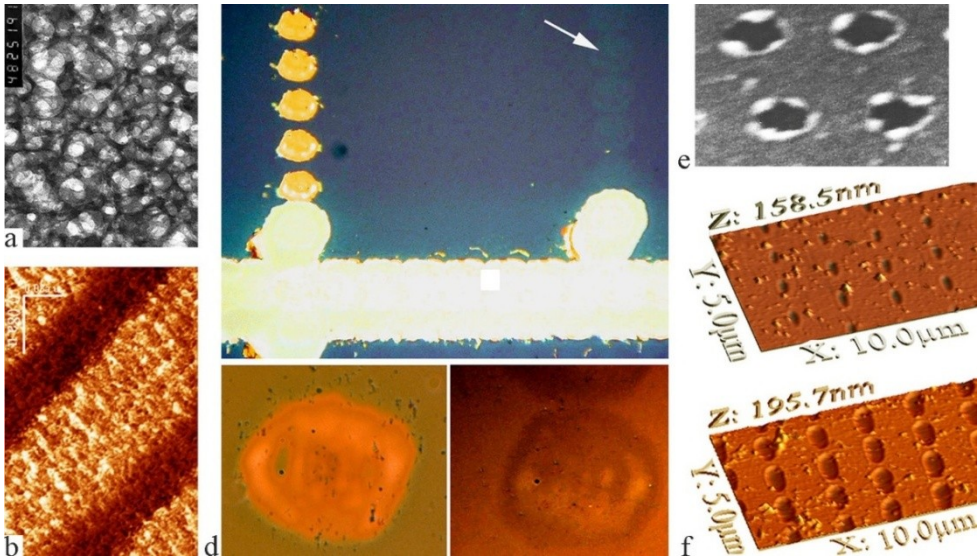

Fig. 3. Morphology of a) Al + PTFE film, b) an electron-beam treated Al + PTFE film, c) excimer laser-treated zones in Au + PTFE film; pits in treated by a focused visible laser beam: e) Au + PTFE and f) dye + PTFE films. Adapted from Ref. [10, 36].

At even lower power densities, only an increase in Au NPs size and their aggregation within the microdomain were observed. AFM studies of microdomains obtained at power densities below the metallization threshold revealed NPs ensembles with sizes and shapes that depend on treatment parameters. In these treated zones, the maximum wavelength of the plasmon band remained unshifted, although the band intensity decreased. Comparison with spectra obtained during thermal annealing suggests that the temperature within the treated domain did not exceed 150 °C. A focused visible laser beam created micrometer-sized holes in a 70 nm dye-filled PTFE film with debris nearly 5 times smaller than that observed in the Au + PTFE film.

Thin PFP films produced through various gas-phase deposition methods are described in [11, 12]. Au NPs were embedded into the Teflon AF matrix. The NC microstructure and metal content are dependent on the deposition rates of the components, the substrate temperature, and the polymer matrix. The size, distribution, and separation

of the Au NPs can be controlled by the deposition parameters. Condensation coefficients, which vary between 0.03 and 1, were determined using energy dispersive X-ray spectroscopy (EDXS). Optical absorption of the films is dependent on the Au filling factor due to the Au NP plasmon band, and a correlation between microstructure and optical properties has been established. A percolation threshold was observed at an Au volume fraction of 0.43 in the Teflon AF matrix. Substrate heating during deposition decreases the condensation coefficient until the glass transition temperature of Teflon AF is reached. Post-deposition heat treatment causes the diffusion of Ag in the Teflon AF, leading to larger Ag NPs sizes, increased interparticle distance, and spheroidal morphology. These changes result in blue shift of the plasmon peak, with temperatures above the glass transition temperature causing a shift toward shorter wavelengths. The morphological evolution of Ag NPs in PFP matrices has been modeled to understand the kinetics of NPs growth [12]. The final microstructure of the film is determined by the competition between the arrival rate of metal atoms and their diffusion on the polymer surface. In aqueous environments, Ag + PFP films exhibit ageing behaviors, where the mobility of Ag atoms leads to changes in the plasmon resonance. Spectro-electrochemical analysis allows for the real-time monitoring of these shifts, providing insight into how the metal-polymer interface reacts under electrochemical bias. A plasmonic meta-material capable of perfect light absorption within the visible spectrum was developed. The fabrication technique yields thin films suitable for flexible substrates, making them ideal candidates for anti-reflector coatings and high-efficiency absorbers. These materials achieve high absorption levels that are largely insensitive to polarization and the angle of incidence. A method for tuning double plasmon resonances involves controlling the dielectric barrier thickness between sandwiched Au and Ag NPs. It was determined that dipole–dipole coupling is strongest at a Teflon AF spacing of 3.3 nm. This geometrical approach to tuning provides higher accuracy for the plasmon resonance frequency than NPs size control. Electromagnetically induced dipole-pair resonance occurs at critical coupling levels, suggesting new pathways for investigating surface-enhanced optical properties involving double plasmon resonances from NPs.

Authors of [13–15] developed a method that combines the deposition of NPs *via* gas aggregation source (GAS) with magnetron sputtering of PTFE. Surface roughness and chemical composition were varied independently. While the PTFE dictates the surface chemistry, the NPs provide the necessary roughness. Results indicate that once a specific surface roughness threshold of 60 nm is reached, the surface transitions to a super-hydrophobic and slippery state. The evolution of 14 nm-sized Ag NPs overcoated by PFP film involves a complex transformation characterized by two distinct regimes. In the early regime, the polymer penetrates the interparticle voids, uplifting the NPs and maintaining a multivalued surface roughness. The presence of the interparticle voids leads to a heterogeneous wetting state with a water contact angle of 135°. Despite the high contact angle, the NC exhibits strong water adhesion, suggesting that the liquid meniscus is located at the lower section of the nanofeatures. In the late regime, the interparticle voids become filled, causing the interface to acquire a single-valued character. As the polymer continues to grow on the roughened surface, the surface displays multi-affinity due to the differing evolution scales of the NPs and the PTFE. The wettability of the film transitions in a homogeneous wetting state [15]. Ag + CFx NC coatings are structured as a three-layer system consisting of a CFx base layer, a central Ag NPs layer, and a CFx top layer. The antibacterial activity of the film is enhanced by increasing the concentration of Ag NPs. These coatings achieve super-hydrophobicity with a water contact angle of 165° and demonstrate biocidal efficacy, capable of inducing a 6-log reduction of bacteria in solution for 4 hours.

Exploration of the evolution of localized surface plasmon resonance (SPR) of Ag NPs as a function of NPs size and dielectric environment was described in [16]. The films were fabricated through the intercalation of dielectric layers – Teflon AF, SiO_2, and TiO_2, which were produced by RF MSp with Ag NPs layers generated via DC MSp. By modulating the DC during deposition, control over the Ag NP dimensions was achieved. Spectroscopy within 350…1100 nm revealed the presence of both dipolar and quadrupolar plasmon resonances, which were interpreted through Mie theory. The morphology of the NPs, characterized via HR-TEM, and their crystalline structure by XRD, established that the optical signature of the NC is a synergistic result of the dielectric constant of the matrix and the size-dependent electronic response of the Ag NPs.

The Ag + PTFE films were produced in [17], where the authors embedded Ag NPs between two PTFE-like layers. The use of separate RF magnetrons for the PTFE and Ag targets allowed for individual control over the deposition of each layer, ensuring that Ag NPs (7 nm) were perfectly encapsulated. The Ag + PTFE films exhibit an absorption peak at 430 nm, attributed to the SPR of the embedded Ag NPs. The intensity of the SPR peak increases with the thickness of the top PTFE layer, which acts as a dielectric host and a barrier against silver oxidation. The inclusion of Ag NPs enhances the refractive index of the NC, reaching values as high as 2.7 at 632 nm. XPS analysis confirmed the formation of chemical bonds (AgC_xFyO_z) at the interfaces, indicating that the plasma promotes chemical interactions that enhance the adhesion and integrity of the NC.

Authors of [18] fabricated films using a ternary CNT/Ag/PTFE composite target *via* mid-frequency dual MSp. A uniform distribution of Ag NPs (6–8 nm in diameter) within a PFP matrix was achieved. The films exhibited high visible light transmittance, exceeding that of the bare PET substrate due to the low refractive index of PFP. These films demonstrated water contact angles reaching 115°, and antimicrobial activity, inhibiting 99.9% of *Staphylococcus aureus* and *Escherichia coli* growth.

The group also prepared Cu-filled PFP NC films using the Cu + PTFE composite targets containing 20, 50, and 80 wt.% Cu. Since targets with 80 wt.% Cu were conductive, sputtering was carried out using both mid-range frequency and DC power sources. Later, the same authors introduced a fabrication method for Cu + plasma PFP NC by employing compression-molded composite targets [19] and achieved precise control over the metal-to-polymer ratio, enabling a transition from dielectric to near-metallic behavior. TEM analysis confirms the formation of spherical Cu NPs (10…20 nm) with a distinct (111) crystalline plane orientation with a lattice distance of 0.208 nm, embedded within the amorphous PFP matrix. The optical response is dominated by SPR, with absorption peaks shifting from 618 nm (mid-frequency power) to 678 nm (DC power) as NP size increases. This red shift correlates with a drop in sheet resistance, down to 34.55 Ω/sq for the DC-sputtered films, producing a highly conductive, red-colored optical filter. The hydrophobicity of PTFE (contact angle ~110°) was reduced by increasing the Cu concentration at the film surface, providing a versatile platform for large-area coatings.

Thin coatings of PTFE + Fe, PTFE + Cu, *etc*., were produced by the authors of the work [20]. The coatings become continuous at a thickness as low as 3 nm. This transition to a continuous film is attributed to the catalytic influence of metallic NPs on the adsorption and polymerization during the deposition. The Fe + PTFE and Cu + PTFE coatings are the PTFE matrix with uniformly distributed metallic NPs ranging from 100 to 200 nm in size. Phase-contrast AFM reveals highly ordered polymer domains surrounding the NPs. Following surface etching in plasma, these regions of ordered polymer reach dimensions of 200 to 300 nm in the PTFE-Fe system. The surface roughness increases proportionally with the metal concentration. Fractal analysis indicates a non-monotonic evolution of the surface dimension, reaching a maximum at a metal-organic compound concentration of 8%. As the concentration increases further, the fractal dimension decreases, which is linked to structuring processes resulting from the coalescence of NPs into Cu clusters. In films containing 20% Cu, IR spectroscopy confirms that the NC formation involves chemical interactions, suggesting the synthesis of Cu-organic compounds. Cu NPs function as nucleation centers for the structuring of the PTFE phase. This molecular ordering is enhanced when coatings are deposited under additional glow discharge (1500 V, 20…60 mA), which optimizes the reactivity of the electron beam evaporation products.

2.2. Titanium–PTFE films

NC films produced by GAS deposition of titanium (Ti) and simultaneous or subsequent plasma polymerization were described in [13–15]. NC were deposited using the GLAD technique and polymer particles as seeds for Ti columnar growth. NPs plasmon resonance was observed in the NC films. The structural integrity of plasma polymers is defined by a disordered, rigid network of short chains characterized by extensive branching and cross-linking. When metallic NPs are incorporated into this matrix, the NC exhibits SPR. For Au NPs, the light color transitions from pink to blue as the filling factor increases from 0.01 to 0.37. The GAS allows for control over the dimensions of NPs by adjusting the residence time in the aggregation chamber and the magnetron current. The size of Ag NPs with 30% of the Al remains in a metallic state. Adjusting the deposition time of NPs, the surface roughness was engineered, which induced hydrophilicity with water contact angles below 5 degrees. The NPs microstructure, alongside the metal fraction, is a defining factor for the electrical resistivity of the film.

Authors of [21] used a stainless steel micromold as an alternative to a silicon micromold in the fabrication of polymeric microfluidic devices. High adhesion and friction of the steel micromold can cause distortion in the microstructure of polymers. Ti, Al, and PTFE were co-sputter deposited on micromolds to improve their surface properties. The sputtering power applied to the PTFE target was varied to control its concentration in the Ti–Al–PTFE films, which affected the bonding structure, surface roughness, friction, and contact angle of coatings. They were characterized using micro-Raman spectroscopy, X-ray photoelectron spectroscopy (XPS), a ball-on-disc tribometer, and a goniometer. The Ti–Al–PTFE coatings were a mixture of carbide, PFP, and amorphous carbon. The surface roughness of coated micromolds decreased with increasing PTFE concentration. The Ti–Al–PTFE coating deposited with 50 W sputtering power on the PTFE target showed the lowest friction coefficient and surface energy of 0.17 and 13.1×10 mN/m, respectively. The coated micromolds showed better replication performance considering the quality of the fabricated polymeric microfluidic devices.

A control over the structural and optical evolution of intercalated PTFE-NiTi NC fabricated *via* RF and DC MSp has been demonstrated in [22]. Investigation on the fabrication, structure, and functional behavior of intercalated PTFE–NiTi NC films was inspired by the combination of soft and hard constituents in natural biological tissues. PTFE was selected for its low surface energy and chemical stability, while NiTi shape memory alloy was chosen for its mechanical robustness, corrosion resistance, and pseudoelastic behavior. PTFE + NiTi NC were fabricated under controlled sputtering conditions, and their microstructural evolution was analyzed using the FTIR, XRD, DSC, TEM, and EDS techniques. At sputtering powers between 50 W and 125 W, a cross-linked PFP network was formed. PTFE chains intercalate within the NiTi lattice without chemical reactions, producing a distinctive microstructure characterized by nanoscale voids, interfacial pits, and polymer chain extension into metallic domains. This intercalation led to changes in surface wettability and friction, with water contact angles approaching ~99° and friction coefficients within 0.1…0.2. Although the thermal incompatibility between PTFE and high-temperature NiTi phase transformation limited the direct activation of shape memory effects, the study establishes a framework for designing NC with tunable tribological and surface properties. At lower pressures, the NiTi NPs maintain a diameter of

10…30 nm, resulting in RMS roughness < 1.5 nm and visible light transmittance of 75…85%. As the sputtering power increases to 125 W, the NPs size grows to 120 nm, leading to a "hilly" topography with a height up to 45 nm. This structural transition allows for the tuning of the refractive index from 1.35 to 1.9.

2.3. PFP films filled with nonmetal NPs

PTFE films filled with Al and ZnS produced by the co-EAVD method were reported in [23]. Al NPs immediately oxidized after air was let into a vacuum chamber. AlO NPs showed an arbitrary shape at a small AlO concentration and a more round shape at high AlO concentrations. The distribution of NPs sizes in the NC film is within the 10…50 nm range (20% vol.% Al) and 70…200 nm (80 vol.% Al). The lines, written in AlO + PTFE film by electron beam in TEM, are shown in Fig. 3b. Al oxide NPs were grown larger, and the distance between them was decreased, while the PTFE matrix was eliminated. Refractive index of the oxidized Al + PTFE films was within 1.34…1.39. PTFE + ZnS films were produced for waveguide sensors.

Authors of [24] developed transition metal difluorides (TMF) + carbon NC films *via in situ* reactive MSp co-sputtering of Fe/Co and PTFE targets, producing binary TMF (FeF_2, CoF_2) NPs with crystallite sizes of 8 nm embedded in a PFP amorphous matrix. The plasma induces decomposition of the PTFE target, releasing fluorine atoms that react with Fe or Co to form dielectric TMF nanocrystals; TEM and XPS confirm a nanogranular architecture with TMF grains isolated by carbon-rich boundaries. The TMF NPs exhibit anti-ferromagnetic behavior with Néel temperatures of 40 K (Co) and 78 K (Fe), establishing TMF+PFP NCs as a platform for investigating disordered antiferromagnets. This inorganic + PFP film provides a high dielectric constant and high transparency, with potential for giant dielectric response and magnetic functionalities. By controlling the PTFE-to-metal ratio, the thermal stability limitations of PFP are overcome, resulting in a transition from a C–F bonded polymer to a TMF ceramic-like NC.

Chalcogenide-bound erbium NPs were embedded into PFP matrices based on hexafluoroisopropyl. PFP is an ideal host because the carbon-fluorine bonds possess lower vibrational frequencies than the carbon-hydrogen bonds in other polymers. By embedding inorganic NPs into PFP, the researchers achieved high optical gain and efficient fluorescence at the 1.5 μm window [25]. The 14*Er*10*S*6*Se*12*I*6 provides a protected environment for the erbium ions, isolating them from any high-energy vibrations. This molecular architecture allows for an absorption cross-section that is larger than that of erbium-doped silicate glasses, enabling more efficient optical pumping and higher gain in shorter path lengths. The ability to process these materials *via* standard co-deposition technique allows for the fabrication of curved waveguides, flexible optical amplifiers, and wearable infrared sensors. By varying the NP-to-polymer ratio, the team identified the optimal doping levels where the material provides maximum optical gain.

Authors of [26] doped PTFE with erbium ions. While PTFE is an insulator with near-infinite resistivity, the incorporation of Er acts as a structural catalyst, transforming the material into a semiconductor. XRD reveals that the dopant forces a massive expansion of the orthorhombic unit cell from 72.66 to 601.85 $Å^3$ indicating a reconfiguration of the polymer chains to accommodate the metallic ions. This structural stress is quantified by the Urbach energy, which rises to 0.58 eV, signaling an intentional increase in disordered states that facilitate charge transport. The material exhibits a tunable bandgap contraction from 5.25 eV down to 4.75 eV, paired with a rise in the absorption coefficient. FTIR spectra confirm the grafting of erbium through the new vibrational mode at 1043 cm^{-1}, shifting the material utility from simple chemical resistance to UV-harvesting and electrical conductivity.

2.4. Oxide-filled fluoropolymer thin films

SiO_x + PTFE films were deposited by RF MSp using argon gas equipped with PTFE and SiO_2 targets in [27]. The composition of the films ranged from PFP with small SiO_x content up to coatings with a greater concentration. The hardness of PFP with increased concentration of SiO_x was 2400 N/mm^2. This is from two to three times higher than for PFP with low SiO content. The static contact angle of water ranges from 112 to 95 deg and the refractive index from 1.49 to 1.43, when the incorporation of SiO_x into the PFP matrix decreases. [40]. The obtained SiO_x/PFP films reveal different wettability (static contact angle of water ranges from 68 to 40 deg.) and hardness (from 720 to 3200 N/mm^2) when the filling factor of SiO_2 changes from 0.01 to 0.7. The concentration of elements determined by RBS/ERDA varies over this range of filling factors. The heterogeneous structure of the NC films is indicated by TEM at high SiO_x contents.

Authors of [28] obtained PTFE + ZnO films with varying ZnO *via* RF MSp. The films exhibited enhanced transmission in the visible range compared to bare ZnO films. A clear UV light cutoff was observed, with a rapid fall below 380 nm and negligible transmission below 300 nm after 10 min of ZnO deposition, which remained unaffected by subsequent PTFE deposition. The absorption edge fell within 300…380 nm, below which the transmission decreased to ~ 0.02%, corresponding to an optical density of 4 for the film deposited for 20 min (total thickness ~ 415 nm) within 200…250 nm. As the ZnO layer thickness increased, the polycrystallinity and surface roughness also increased, leading to changes in crystallite orientations and grain distribution on the film surface. AFM analysis revealed island-like growth, resulting in a mixed ZnO + PTFE layer. Surface roughness was ~ 8…9 nm for both lower and higher thicknesses, except for the film in which a continuous layer appeared to have formed. A layer model was developed consisting of a glass substrate, an oxide SiO_2 layer, a dense ZnO layer, followed by a PTFE + ZnO mixed layer, and finally covered by a PTFE layer. By choosing appropriate layer thicknesses and number of layers, such

thin films could potentially be used as antireflection coatings with UV protection below 400 nm.

Authors of [29] prepared coatings composed of ZnO NPs in PFP matrix by ion beam sputtering (IBS) of ZnO and PTFE targets. Tuning IBS parameters, the NPs load was controlled, thus modulating the antibacterial/antistain/antifouling properties. The coatings were characterized by AFM and TEM to obtain information on the material surface composition, nanocoatings morphology as a function of the ZnO loadings. XPS spectra evidenced a high degree of polymer defluorination along with the formation of inorganic fluorides at increasing ZnO volume ratios. Post-deposition treatments for fluorides removal were performed directly in the deposition chamber. A complete stoichiometry for inorganic NPs was obtained, allowing for the conversion of fluorides into ZnO.

Al_2O_3-filled PTFE coatings were developed by the authors of [30]. The surfaces of artificial joints are susceptible to premature wear, which reduces their service life, leading to the increased risk of revision arthroplasty. Tribological coatings having low coefficients of friction and which are biocompatible are therefore required to minimize such risks. PTFE + Al_2O_3 thin coatings were prepared by MSp and incorporated with cold-sprayed NCs to extend the service life of artificial joints. Surface analysis indicated the formation of a PFP+Al_2O_3 NC. This film exhibited excellent friction-reducing ability up to an applied load of 7 N. Regardless of whether the Ti–6Al is manufactured by a layer-by-layer or co-sputtered, the coefficient of friction is reduced to below 0.1 at the start of the test. The PTFE + Al_2O_3 film functionalizing the cold-sprayed surface is reliable for devising material systems operating in high-wear applications.

Developed by authors of [31], flexible and transparent antimicrobial touch sensors have received attention on account of their wider applicability in personal electronic devices. Anti-reflective, hydrophobic, antimicrobial ZnO + PTFE thin films with sensorial capabilities were produced *via* MSp. The ZnO + PTFE film exhibits a low refractive index, high transmittance, and excellent hydrophobic properties, along with antibacterial activities. Zinc dissolution in water from the ZnO was prevented by compositing with PTFE to realize long-term water stability and mechanical durability of ZnO films. A triboelectric nanogenerator (TENG) based antimicrobial self-powered touch sensor that delivered recordable pressure/touch sensitivity is developed based on ZnO + PTFE films. The ZnO + PTFE-based TENG is shown to provide a high triboelectric output voltage of 224 V, a current density of 21.4 mA·cm^{-2}, and a power density of 1.65 mW·cm^{-2}. The linear response of the TENG to driven pressure indicates its pressure-sensing ability, with a sensitivity of 75.31 V·kPa^{-1} and a touch sensitivity of 31.36 V·kPa^{-1}. The application of ZnO + PTFE as a display coating and self-powered touch sensor is demonstrated.

Using the density functional theory (DFT), authors of [32] have modeled the surface modifications of PTFE with two metal oxides, SiO_2 and ZnO, individually and as a mixture of these two. The B3LYPL/LANL2DZ model was used to follow up on the changes in electronic properties. The total dipole moment (TDM) and HOMO/LUMO band gap energy (ΔE) of PTFE, which were 0.000 Debye and 8.517 eV, respectively, were enhanced to 13.008 Debye and 0.69 eV in the case of TFE/4 ZnO/4 SiO_2. With increasing the filler PTFE /8 ZnO/8 SiO_2, TDM changed to 10.605 Debye, and ΔE decreased to 0.273 eV, leading to improvement in the electronic properties. The molecular electrostatic potential and quantitative structure-activity relationship studies revealed that modification of PTFE with ZnO and SiO_2 increased its electrical and thermal stability. The improved PTFE/ZnO/SiO_2 NC can be used as a self-cleaning layer for astronaut suits.

3. Dye-filled and dye-metal-filled PFP thin films

3.1. Dye-filled PTFE films

The structural instability of small-molecule organic semiconductors remains a primary obstacle to their industrial longevity. Molecules of these materials, which are integral to the next generation of organic light-emitting diodes (OLEDs) and organic photovoltaics, are held together by weak van der Waals interactions. Under thermal stress generated by device operation or the external environment, the soft matter comprising these molecules undergoes diffusion and crystallization, leading to degradation of the film electrical performance. The first hybrid films were produced by co-deposition of phthalocyanine (Pc) and PTFE [33–37] by Grytsenko with co-authors, and the H_2Pc, CoPc, ZnPc, and VOPc were used to fill the PTFE matrix. Farther, Grytsenko with his co-authors, produced PTFE films filled with dyes of various types. Optical spectra of dye + PTFE films are presented in Fig. 4. The optical properties of the films exhibit a strong dependence on both the dye structure and its concentration within the PTFE matrix. VOPc-filled films demonstrate the most significant spectral modifications. While pure VOPc films deposited by PVD show three absorption maxima at 655, 720, and 820 nm, the incorporation into PTFE alters these transitions. In as-deposited composite films, the 820 nm peak remains unresolved, and the intensity of the 720 nm band undergoes a more pronounced reduction compared to the 655 nm peak. Thermal treatment for 10 hours does not restore the 825 nm band, showing that the PTFE matrix stabilizes the VOPc NPs. The suppression of the 825 nm band intensity is directly proportional to the PTFE concentration, indicating that the polymer matrix and the application of RF-discharge hinder the aggregation of dye NPs. As a result, these NC films demonstrate enhanced thermal stability compared to pure dye films.

The chemical structure of the dyes determines their aggregation within the PTFE matrix. PTFE films containing dye 1 (Fig. 4c, the dye's name is indicated in the caption) maintain an absorption maximum close to that observed in solution. Similar spectral stability is observed for dye 2 (Fig. 4c), and dye shown in Fig. 4d. Hydroxy-squaraines in PTFE (Fig. 4e, 4f) display concentration-dependent spectral changes, including the

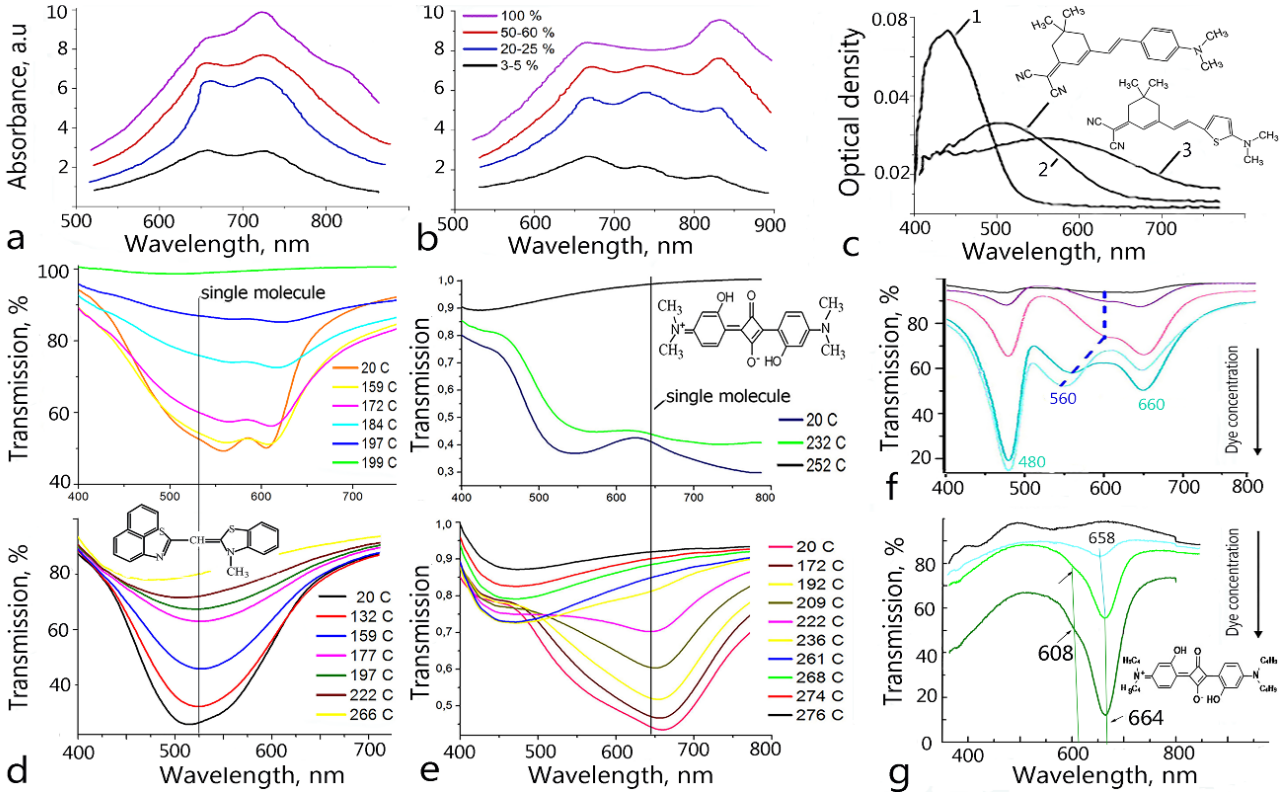

Fig. 4. Optical spectra of thin dye-in-PTFE films various concentrations of dyes: a) as-deposited VOPc-in-PTFE, b) VOPc-in-PTFE after annealing in air; copied from [33], c) three similar dyes: 1) 2-{3-[2-(4-methoxy-cyclohexyl)-vinyl]-5,5-dimethyl-cyclohex-2-enylidene}-malononitrile; 2) 2-{3-[2-(4-dimethylamino-cyclohexyl)-vinyl]-5,5-dimethyl-cyclohex-2-enylidene}-malononitrile and 3) 2-{3-[2-(5-dimethylamino-thiophen-3-yl)-vinyl]-5,5-dimethyl-cyclohex-2-enylidene} malononitrile in PTFE matrix; copied from [34], d) annealing in air of 2-(benzo[cd]indol-2-ylmethylene)-3-methyl-2,3-dihydrobenzo[d]thiazoleand OHSq1: upper – pure dye film, down – in PTFE matrix. e) annealing in air of dihydroxy-substituted bis(dimethylamino)squaraine in PTFE with low concentration: upper – pure dye film, down – in PTFE matrix. f) this dye in PTFE with various concentrations; g) butyl-substituted Sq in PTFE with different concentrations. Adapted from Ref. [4, 33, 34].

emergence of a new band at 480 nm and variations in shoulder splitting at 603 and 660 nm. These effects confirm that while the PTFE matrix promotes initial dye-dye interaction due to weak dye-polymer affinity, it simultaneously acts as a barrier preventing the growth of larger dye NPs. The photochromic performance of spiropyran-in-PTFE films highlights the protective role of the matrix. Initial films show a UV absorption band at 360 nm, with a minor visible band corresponding to the merocyanine form. UV irradiation triggers a sharp increase in visible absorption, a behavior consistent with other spiropyran-polymer systems [35]. The PTFE matrix provides superior resistance to irreversible photo-chemical degradation compared to PMMA matrices under identical irradiation conditions. The results cannot be explained simply as the sum of the dye and PTFE properties. Gas diffusion through such thin films should occur within a few seconds. The PTFE films contain a negative electric charge [36], which may prevent gas molecules from penetrating the film bulk. However, the mechanism underlying the suppression of phototrans-formations of the spiro-compounds, as well as the unique properties of NP-filled films in a charged PTFE environment, remains unclear [37].

The films produced by co-evaporation of the dye 4,40-bis[N-(1-naphthyl-1)-N0-phenyl-amino]-biphenyl with Teflon AF were obtained in [38]. At a concentration of 25 vol.% of the Teflon AF, the polymer creates an interpenetrating network that encapsulates the organic molecules. This network inhibits the aggregation of dye molecules. The operating temperature limit increased beyond 250 °C. This mixing does not compromise charge transport; in fact, in the NC, the drive voltage in single-layer hole-only devices was improved by 30%. This suggests that the low-energy surface of the Teflon AF chains may assist in reducing interfacial traps or maintaining a more favorable molecular orientation for hopping transport, providing a robust pathway for the tuning of thermal and optical properties of the films.

Authors of [39] reported a methodology for improving the photosensitivity of organic photodiodes through the mixing of the PTFE with organic semicon-ductors. Heterostructures based on ZnPc and fullerenes were produced by co-evaporation with PTFE. A new photocurrent amplification mechanism within films ZnPc-C70 + PTFE was proposed. This effect is attributed to the formation of stable NPs 5…30 nm within the PTFE matrix, which increases the donor-acceptor

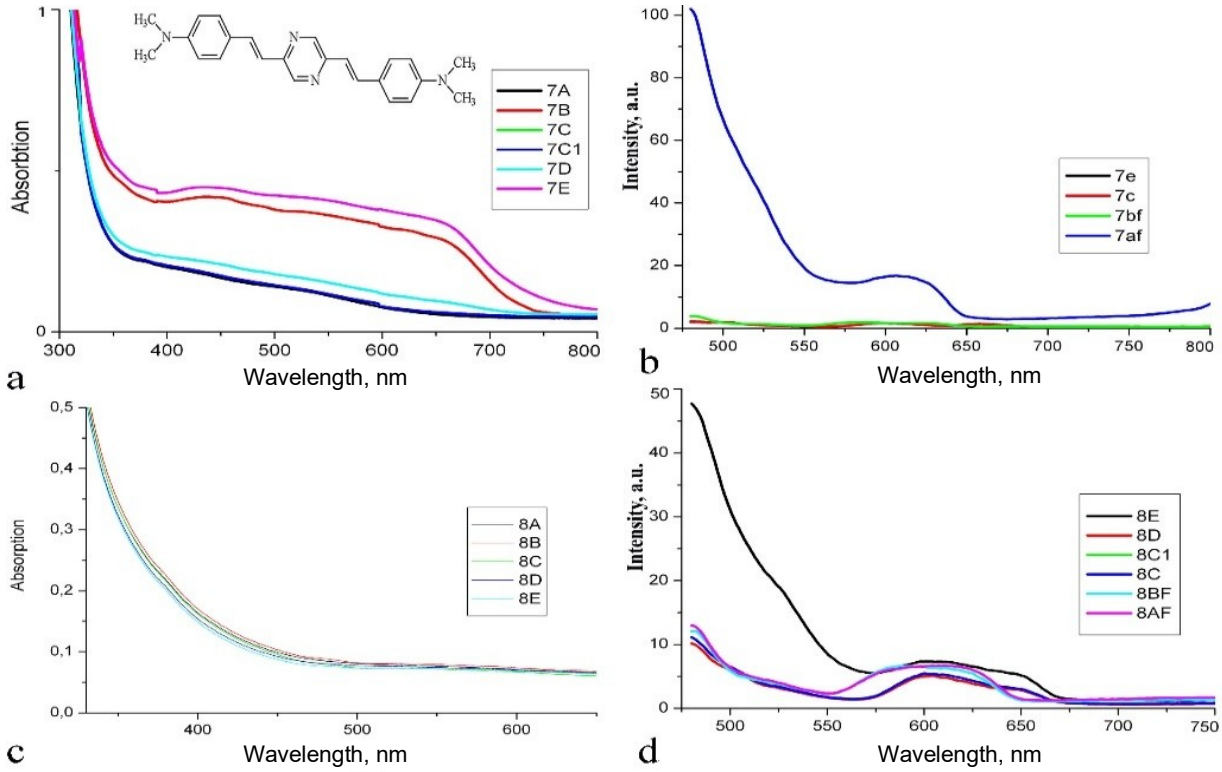

Fig. 5. Spectra changes of the NC films after vapor treatment: a) absorption and b) luminescence of the dye + Au + PTFE film; c) absorption and d) luminescence of the dye + As_2S_3 + PTFE film. Adapted from Ref. [37].

interface area, thereby facilitating exciton dissociation and charge carrier generation. Nc film shows a sensitivity increase exceeding 100%. C70 + PTFE device achieved a peak sensitivity of 0.13 A/W under bias + 0.67 V, which is only 2.3 times lower than the sensitivity of silicon photodiodes. Dielectric spectroscopy revealed that the NC film ZnPc + PTFE reduces the dielectric loss tangent by nearly one order of magnitude, indicating a suppression of trap-assisted dark conductivity and noise. The films exhibited exceptional thermal resilience, maintaining their morphological integrity up to 260 °C. The PTFE-based films in heterojunction showed the external photosensitivity 20 times bigger than that of ZnPc films following the same storage period.

Co-evaporation of a hole transport material with Cytop (poly-perfluorobutenyl vinyl ether) was used for refractive index modulation of NC film [40]. A nano-sized pillar-like two-phase thin film was produced. During the deposition process, vertically oriented channels of the HTM (4,40,400-tris[2-naphthyl(phenyl) amino]triphenylamine) formed in the Cytop matrix. The characteristic scale of this phase separation is less than 50 nm, which is below the sub-wavelength threshold. This structural refinement suppresses Rayleigh scattering, maintaining high optical transparency and ensuring that the composite layer functions as a single optical medium. By adjusting the volume fraction of the Cytop, the refractive index of the NC layer at 550 nm was reduced from 1.81 to 1.56. The extinction coefficient remains below 10^{-4}, indicating negligible absorption losses across the visible spectrum. This reduction in the refractive index to 1.5 optimizes light outcoupling at the anode ITO/organic interface. Optical modeling and experimental verification indicate that the lowered refractive index redistributes the mode density, suppressing waveguide modes within the organic stack and increasing the fraction of outcoupled light. The implementation of low-index layers within phosphorescent OLED resulted in a 1.22-fold (22%) increase in external quantum efficiency. Despite the introduction of polymer, the current density-voltage characteristics exhibited minimal deviation. At a current density of 10 mA/cm^2, the operating voltage increased by only 0.1…0.2 V. This confirms the efficacy of the pillar-like architecture in maintaining continuous charge transport pathways.

3.2. Dye + metal-filled polymer films

PTFE and PPS films filled simultaneously with dye and metal NPs were produced by the authors of [37, 41, 42]. The PTFE matrix is better in PPS, which maintains the monomeric state of embedded dye molecules. While squaraine molecules in the PPS matrix tend to aggregate, with these aggregates decomposing at temperatures near the dye decomposition point, PTFE suppresses aggregation even at dye concentrations up to 30%. The PTFE + dye films are inert to external chemical triggers, including trifluoroacetic acid vapors, which can be due to the electric charge trapped within the PTFE [36]. Fig. 5 presents the optical spectra changes after vapor treatment. The introduction of NPs of a third inorganic phase alters the films responsiveness. In the dye + Au + PTFE films, the

inorganic NPs act as adsorption sites that facilitate the transport of gaseous molecules into the PTFE film, thereby enabling optical sensing of vapors. This mechanism overcomes the barrier properties of the PTFE matrix, allowing for the development of robust, protected sensors where the dye luminescence or absorption spectra can be modulated by external chemical agents.

The films consisting of Au NPs embedded in PTFE or cellulose acetate matrices by co-deposition were presented in [41–43]. The method allows for the simultaneous or sequential evaporation of the metal and the polymer, alongside additives such as calixarenes and dyes. Au NPs within the dielectric host were formed, where the Au NPs provide electrical conductivity *via* the electron percolation/tunneling mechanism. The organic molecules modify the inter-particle spacing and the local chemical environment, which is critical for tuning the sensor's response. The conductivity is sensitive to the dye's interaction with external analytes, which induces electronic changes in the NC film. The sensing principle is based on the relative resistance variation, which reaches 10…15% upon exposure to organic vapors. The presence of the Au NPs allows for a percolating conductivity that is modulated by the molecular absorption of analytes into the polymer layer. By incorporating specific organic molecules, the selectivity profiles of the Au + PTFE sensors can be altered, enabling the recognition of different chemical species. Based on these sensitive coatings, the authors developed chemoresistive sensors in which Au NPs are embedded in a PTFE or PPS matrix. These sensors employ a system of 20 pairs of Au raster electrodes fabricated on ceramic substrates. The sensing mechanism relies on percolation conductivity between Au NPs dispersed within the organic matrix. Upon exposure to analyte vapors, the organic matrix undergoes swelling, which increases the distance between neighboring Au NPs and results in a change in electrical resistance. Dye + Au + PTFE and iodine + Au + PTFE films were prepared using EAVD co-deposition. The incorporation of dye or iodine introduces new energy states that alter the conduction mechanism and even reverse the sign of the sensor response. NC, based on PTFE, exhibits greater chemical and thermal stability than calixarene-based films. The relative responses of the chemoresistor reach levels of 15…20%. The ability to tailor chemosensitivity offers broad prospects for the development of chemical recognition systems.

4. Thin films for biomedical applications

NCs with Ag NPs embedded in plasma polymer matrices, including PTFE-like, were produced in [15, 43]. Gas aggregation source was used to produce Ag NPs with controlled size. These composites exhibit distinct optical properties through SPR, which can be tuned by adjusting the thickness of the PTFE-like overcoat or the NPs filling factor. The antimicrobial performance is exceptional, with Ag + PTFE-like coatings achieving a 7-log reduction in *Staphylococcus aureus* populations. Despite the hydrophobicity of PTFE, layers of about 10 nm still allow for effective Ag^+ ion leaching through structural microdefects. Adding a 1% of gold to the Ag NPs increased the ion release rate by one order of magnitude due to galvanic coupling. These PTFE-based systems demonstrate durability, maintaining their antibacterial effect against *E. coli* after 10,000 washing cycles. Such coatings can provide a sustained release of biocidal agents for a period exceeding 300 days.

Produced Ag + CFx nanocomposites were reported in [44]. Ag NPs with a diameter of 5…7 nm are dispersed within a PFP matrix. SEM used to map the release of Ag^+ ions, revealing that even at a silver content of 4.4 at.%, the matrix provides sustained ion elution. The films exhibit a SPR peak centered at 430 nm, which serves as a signature of the metallic state of the embedded NPs. *P. fluorescens* biofilm formation was inhibited, showing that the biocide-releasing surface prevents bacteria from transitioning to a mature sessile state within the first 24 to 48 hours. The silver release reaches a steady-state concentration of 0.35 μg/cm^2 after the initial immersion phase. The presence of the PFP matrix doubles the lifespan of the antibacterial effect compared to bare Ag, as it regulates the oxidation of the 5 nm particles. AFM and IR showed that bacteria in contact with the surface undergo biochemical stress, leading to a reduction in protein and polysaccharide signals. The cyclic changes in the IR bands correlated with the stress of bottom-layered bacteria, along with re-colonization on top of dead biomass, indicative of cannibalism.

Authors of [45] present a multilayer NC where Ag and silver oxide NPs with diameters from 15 to 30 nm were embedded in a CFx matrix with 12 at.% Ag. By adjusting the plasma duty cycle (5.3% to 20%), the F/C ratio was controlled from 0.8 to 1.3. The system is characterized by a low surface energy of 8.3 to 13 mN/m and a water contact angle of 122.8°, which creates a hostile environment for bacteria. The antimicrobial performance achieved an 88% inactivation rate for *E. coli* and inhibited biofilm formation during the 12 hours of exposure. The 50 nm thick CFx layer acts as a diffusion barrier, preventing the initial “burst” of ions and ensuring that Ag release remains below the human cytotoxicity.

Ag NPs in PFP films prepared *via* the combination of a GAS and initiated chemical vapor deposition (iCVD) were described in [46]. The iCVD utilizes the perfluoro-butane sulfonyl fluoride or similar precursors, maintained at a partial pressure of 10 to 30 Pa during film growth. A heated filament array, operating at a temperature from 250 to 300 °C, decomposes the initiator (TBPO) to trigger radical polymerization on a cooled substrate held at 20 °C. Simultaneously, the GAS source generates Ag NPs in the gas phase using MSp with a power of 20 to 50 W. Argon gas at a flow rate of 20 to 80 sccm acts as the carrier, facilitating the formation of NPs with diameters ranging from 5 to 20 nm. The films with metal filling factor, reaching up to 40% by volume without compromising the chemical integrity of PTFE, were obtained. XPS showed a CF_2 content of over 60%. The deposition rate of the NC

is controlled at 1 to 5 nm/min to ensure a uniform distribution of NPs. Field-emission scanning electron microscopy revealed a high density of Ag NPs embedded throughout the 100-nm-thick film. These NC exhibit superior antibacterial properties, reducing colony-forming units by 99.9% within 24 hours. TEM showed that the Ag NPs maintain a crystalline structure with a lattice spacing of 0.23 nm, characteristic of the (111) plane. The PFP matrix provides mechanical stability, preventing the leakage of metal ions into the environment.

Polymer films filled with an antibiotic by the method of electron beam decomposition-evaporation of a mixture of polymer and ciprofloxacin were formed in [47]. Polymer matrix controls the release of the ciprofloxacin in an isotonic sodium chloride solution. For the coatings with Ag NPs, the antibacterial action on drug-resistant bacteria was defined. The worn-out areas of the coating after 17 and 25 wear cycles were 47% and 53%, respectively. Standard sterilization heat treatment of the coating does not affect the kinetics of the release of ciprofloxacin. Microbiological studies showed high antibacterial activity of the NC layer in relation to *P. aeruginosa* and *E. coli*.

Authors of [48, 49] reported on films co-deposited from 316L stainless steel and PTFE *via* RF MSp onto vascular stents and neural implants, thus modifying the surface morphology and chemical functionality. According to in-depth XPS analysis, the fluorine concentration in these layers varies from 11 to 57 at.% depending on the deposition parameters. TEM showed that iron fluoride (FeF_2) crystallites, densified by the (211) plane, are embedded within an amorphous PTFE. This structural gradation eliminated stress concentrations, as evidenced by nanoindentation tests where mechanical properties converge at a critical load of 0.7 mN. This allowed a fast re-endothelisation of the coated stent. Antimicrobial efficacy is achieved by doping the organic/inorganic matrix with Ag. The co-deposition of Ag with hydroxyapatite and PTFE creates a surface characterized by an inhomogeneous phase distribution. This feature induces a dual-functional response, promoting healthy cell integration and inhibiting the growth of pathogenic bacteria. The PTFE top layer prevents protein denaturation, preserving the 3D conformation of adsorbed bovine serum albumin. Structural stability is maintained even at high polymer concentrations, ensuring that the antimicrobial dopants do not leach rapidly into the surrounding tissue. The hybrid nature of the film also allows for enhanced imaging capabilities, as elements like Au can be incorporated to increase electronic density. The transition from metallic to ionic/covalent bonding across the gradient ensures that the antimicrobial surface is anchored to the metallic substrate. Recent data indicate that such graded antimicrobial surfaces significantly reduce biofilm formation. The review [49] analyzes polymeric coatings designed to combat pathogens like *S. aureus* and *E. coli*. Antimicrobial effects are achieved through surface topography, where nanopillars (200 nm in height) reduced bacterial adhesion by 40…70%. The integration of Ag NPs at concentrations of 1 to 5 wt.% is shown to achieve a 99.9% reduction in microbial viability. ZnO coatings create inhibition zones of 10 to 18 mm against *S. aureus,* depending on the polymer matrix. Copper-loaded polyurethane coatings provided complete sterilization against *E. coli* within 60 min of contact. Photocatalytic coatings using TiO_2 can eliminate 10^6 cells/mL under UV light 1 mW/cm^2. Antiviral SARS-CoV-2 Spike-ACE-2 binding inhibition reaches 65% of Ag NPs. The NC improves the apoptotic gene expression for liver cancer cells.

Investigation of graded PFP films prepared *via* electron- and ion-assisted vapor deposition polymerization is provided in [50]. Fluoropolymer films are synthesized using 2-(perfluorohexyl) ethylacrylate monomers under Ar ion irradiation. The ion acceleration voltage (Va) is a critical parameter: increasing Va from 0 to 500 V improves the adhesion strength between the film and the glass substrate and increases the surface energy and the refractive index. To resolve these conflicting requirements, a graded film is prepared by varying Va from 300 to 0 V during the film growth. This gradient structure allows for high-energy "anchoring sites" at the substrate interface while maintaining a low surface energy of 8.5 mJ/m^2 at the outer surface. The graded film acts as an efficient antireflective coating, reducing the optical reflectivity of the glass from 4.9% to 0.55% at 400 nm. The refractive index is controlled by the ion bombardment, with values at 546 nm ranging from 1.368 at 0 V to 1.395 at 300 V. The adhesion of the graded film is verified through sonication in water and immersion in HCFC-225, demonstrating stability against organic solvents and mechanical stress that fixed low-voltage films cannot withstand. This graded approach eliminates the need for limited halogenated solvents or brittle inorganic multilayers. The variation of Va during deposition is a versatile method for creating ductile, adherent, and high-performance optical coatings.

The review [51] summarizes the results of using the EAVD method to obtain thin polymer films, which allows the engineering of functionally gradient structures. This enables the transformation of material properties, such as increasing the pencil hardness of Teflon AF from a soft 10B monomeric state to a robust 4H cross-linked polymer network. By initiating deposition at high energy, superior interface adhesion was achieved, while a subsequent reduction in Va yields a surface energy as low as 6.0 mN/m for Rf-10 acrylate films. These graded films suppress optical reflection by smoothing the refractive index transition from 1.35 to 1.38 throughout the film thickness. For two-component systems, vapor-deposition polymerization requires a rigorous 1:1 stoichiometric ratio of co-evaporated monomers, such as diamines and diisocyanates, to ensure high molecular weight polyurea formation. The EAVD process facilitates simultaneous polymerization and dipole orientation by utilizing an electron current of 10 mA to generate an internal electric field during growth. In high temperature variants, partial pressures can be increased to

0.1 Pa to achieve conformal multicomponent coatings on three-dimensional geometries. Ternary systems are developed for OLEDs, where a host matrix is co-deposited with multiple dopants to optimize energy transfer pathways. Radical polymerization of multicomponent acrylates *via* EAVD achieves a polymer conversion rate of 96%. The EAVD method allows for the integration of incompatible functional units, such as carbazole or naphthalenediimide, as pendant groups within a 100 nm thick composite layer. Molecular layer deposition enables the sequential supply of different monomers to build multicomponent structures with monolayer precision. Ion irradiation during these processes can control the in-plane molecular orientation, enhancing charge carrier mobility in organic semiconductors. The multicomponent films demonstrate enhanced thermal stability, with glass transition temperatures higher than those produced *via* spin-coating.

5. Conclusion

The review presents the methods of fabrication, physical properties, and application area of thin nanocomposite films based on perfluoropolymers, and considers the development trends in this field. The advantages of perfluoropolymer matrices for protecting metal nanoparticles from corrosion, providing surfaces with superhydrophobic properties, extending the service life of medical implants, improving the characteristics of functional layers in organic light-emitting diodes, sensor sensitive elements for biomedical applications are demonstrated. It is shown that metal nanoparticles and dyes included in the composition of perfluoropolymer matrices exhibit unique optical properties, and organic molecules embedded in such matrices demonstrate exceptional stability, making these materials promising for use in optics, sensors, and biomedicine.

Acknowledgements

This work was supported by the National Academy of Sciences of Ukraine in the framework of the implementation of the project “Creation of basic technologies for forming semiconductor materials and structures for nano- and optoelectronics” (project No. III-10-24).

References

1. Dilks A., Seybold D. Metal-containing fluoropolymer films, produced by simultaneous plasma etching and polymerization. *J. Appl. Phys.* 1980. **51**, No 11. P. 5678–5687. https://doi.org/10.1063/1.327491.
2. Usui H. Physical vapor deposition of polymer thin films. *Jpn. J. Appl. Phys*. 2025. **64**, No 3. 030802. https://doi.org/10.35848/1347-4065/adb439.
3. Grytsenko K. Polymeric metal-filled films for photothermal optical recording. *Proc. SPIE.* 1997. **3347**. 165–173. https://doi.org/10.1117/12.301405.
4. Grytsenko K.P., Krasovsky A.M. Thin film deposition of polymers by vacuum degradation. *Chem. Rev.* 2003. **103**, No 9. P. 3607–3650. https://doi.org/10.1021/cr010449q.
5. Miyake S., Shindo T. Deposition and tribological properties of multilayer and mixed films composed of gold and polytetrafluoroethylene. *TSF.* 2013. **527**. P. 210–221. https://doi.org/10.1016/j.tsf.2012.12.019.
6. Wei H., Eilers H. Electrical conductivity of thin-film composites containing silver nanoparticles embedded in a dielectric teflon AF matrix. *TSF*. 2008. **517**, No 2. P. 575–581. https://doi.org/10.1016/j.tsf.2008.06.093.
7. Grytsenko K., Capobianchi A., Convertino A. Polymer-metal composite thin film prepared by co-evaporation in vacuum, In the book: *Polymer Surface Modification and Polymer Coatings by Dry Process Technologies*, Ed. S. Iwamori. Research Signpost, Kerala, 2005. P. 85–109.
8. Grytsenko K. Tuning of the optical properties of gold nanocluster ensemble formed in polytetrafluoroethylene film. *Opt. Mem. Neural Netw.* 2009. **18**, No 4. P. 290–294. https://doi.org/10.3103/s1060992x09040079.
9. Grytsenko K., Kolomzarov Y., Lytvyn P. *et al.* Optical and Mechanical Properties of Thin PTFE Films, Deposited from a Gas Phase. *Macromol. Mater. Eng.* 2023. **308**. 2200617. https://doi.org/10.1002/mame.202200617.
10. Grytsenko K., Kolomsarov Yu., Belyaev O., Schrader S. Protective applications of vacuum-deposited perfluoropolymer films. *SPQEO*. 2016. **19**. P. 139–148. https://doi.org/10.15407/spqeo19.02.139.
11. Takele H., Schurmann U., Greve H. *et al.* Controlled growth of Au nanoparticles in co-evaporated metal/polymer composite films and their optical and electrical properties. *Eur. Phys. J. Appl. Phys.* 2006. **33**. P. 83–89. https://doi.org/10.1051/epjap:2006006.
12. Takele H., Kulkarni A., Jebril S. *et al.* Plasmonic properties of vapour-deposited polymer composites containing Ag nanoparticles and their changes upon annealing. *J. Phys. D: Appl. Phys*. 2008. 41. P. 1–6. https://doi.org/10.1088/0022-3727/41/12/125409.
13. Petr M., Kylián O., Kratochvíl J. *et al.* Nanocomposite metal/plasma polymer films deposited by gas aggregation sources of nanoparticles combined with magnetron sputtering of polymers. *22nd Symposium on Plasma Chemistry*, University of Antwerp, Belgium, July 5-10, 2015.
14. Choukourov A., Kylian O., Petr M. *et al.* RMS roughness-independent tuning of surface wettability by tailoring silver nanoparticles with fluorocarbon plasma polymer. *Nanoscale.* 2017. **9. P.** 2616–2625. https://doi.org/10.1039/c6nr08428a.
15. Kylian O., Kratovich J., Petr M. *et al.* Ag/C:F Antibacterial and hydrophobic nanocomposite coatings. *Funct. Mater. Lett.* 2017. **10**. P. 1750029. https://doi.org/10.1142/s1793604717500291.
16. Tafur G., Benndorf C., Acosta D. *et al.* Optical properties of silver nanoparticles embedded in dielectric films produced by dc and rf magnetron sputtering. *IOP Conf. Series: J. Phys.* 2019. **1173**. P. 012004. https://doi.org/10.1088/1742-6596/1173/1/012004.

17. Satulu V., Mitu B., Ion V. *et al.* Combining fluorinated polymers with Ag nanoparticles as a route to enhance optical properties of composite materials. *Polymers*. 2020. **12**. P. 1640. https://doi.org/10.3390/polym12081640.
18. Cho E., Kim S., Kim M. *et al.* Super-hydrophobic and antimicrobial properties of Ag-PPFC nanocomposite thin films fabricated using a ternary carbon nanotube-Ag-PTFE composite sputtering target. *Surf. Coatings Technol.* 2019. **370**. P. 18–23. https://doi.org/10.1016/j.surfcoat.2019.04.045.
19. Kim S., Kim M., Park J.S., Lee S. Optical, electrical, and surface properties of Cu/plasma polymer fluorocarbon nanocomposite thin film fabricated using metal/polymer composite target. *Appl. Sci.* 2019. **9**. P. 1296. https://doi.org/10.3390/app9071296.
20. Rogachev A., Yarmolenko M., Rahachou A. *et al.* Structure and properties of nanocomposite polymer coatings. *J. Phys. Conf. Series.* 2008. **100**. P. 082042. https://doi.org/10.1088/1742-6596/100/8/082042.
21. Saha B., Tor S.B., Liu E. *et al.* Titanium–aluminum–PTFE steel micromold *via* co-sputtering deposition: Replication performance and limitation in hot-embossing. *Sens. Actuators B.* 2012. **163**. P. 290–298. https://doi.org/10.1016/j.snb.2011.12.096.
22. Anjum S. PhD Theses: *Fabrication of Smart Intercalated Polymer – SMA Nanocomposite.* Cranfield University, UK, 2014.
23. Grytsenko K., Sopinski M., Convertino A. *et al.* Electrical and optical waveguide sensors, exploiting PTFE film, filled with organic and inorganic nanoclusters. Abstr. Book: E-MRS Spring Meeting, May 29–June 3, Strasbourg, 2007.
24. Cao Y., Nogawa K., Kobayashi N., Masumoto H. Fabrication of transition metal difluorides–carbon nanocomposite films by magnetron co-sputtered deposition of Fe/Co and Teflon targets. *Appl. Phys. Express.* 2021. **14**. P. 075502. https://doi.org/10.35848/1882-0786/ac07f0.
25. Kumar G.A., Riman R., Banerjee S. *et al.* Infrared fluorescence and optical gain characteristics of chalcogenide-bound erbium cluster-fluoropolymer nanocomposites. *Appl. Phys. Lett.* 2006. **88**. P. 091902. https://doi.org/10.1063/1.2170433.
26. El Moutarajji A., Tbib B., El-Hami K. Effect of erbium addition on optical and electrical properties of polytetrafluoroethylene. In: *Advanced Intelligent Systems for Sustainable Development* (AI2SD'2018), Ed. M. Ezziyyani. 2019. P. 97–110. https://doi.org/10.1007/978-3-030-12065-8_10.
27. Pihosh Y., Biederman H., Slavinska D. *et al.* SiO_x/fluorocarbon plasma polymer films prepared by magnetron sputtering of SiO_2 and PTFE. *Vacuum.* 2006. **81**. P. 38–44. https://doi.org/10.1016/j.vacuum.2006.02.007.
28. Tripathi S., De R., Rao K. *et al.* Thickness-dependent optical and structural properties of polytetrafluoroethylene/zinc oxide films by radio frequency magnetron sputtering. *Adv. Polym. Technol.* 2018. **37**. P. 2774–2787. https://doi.org/10.1002/adv.21950.
29. Sportelli M.C., Valentini M., Picca R. *et al.* New Insights in the ion beam sputtering deposition of ZnO-fluoropolymer nanocomposites. *Appl. Sci.* 2018. **8**. P. 77. https://doi.org/10.3390/app8010077.
30. Ng C., Rao J., Nicholls J. The role of PVD sputtered PTFE and Al_2O_3 thin films in the development of damage tolerant coating systems. *J. Mater. Res. Technol*. 2020. **9**. P. 675–686. https://doi.org/10.1016/j.jmrt.2019.11.009.
31. Ippili S., Jella V., Lee J. *et al.* ZnO–PTFE-based antimicrobial, anti-reflective display coatings and high-sensitivity touch sensors. *J. Mater. Chem. A*. 2022. **10**. P. 22067–22079. https://doi.org/10.1039/d2ta06095g.
32. Ezzat H.A., Hegazy M.A., Ghoneim R. *et al.* DFT and QSAR studies of PTFE/ZnO/SiO_2 nanocomposite. *Sci. Rep.* 2023. **13**. P. 9696. https://doi.org/10.1038/s41598-022-19490-0.
33. Grytsenko K., Dimitriev O., Kisluk V. *et al.* Dye-fluoro-polymer nanocomposite film deposition in vacuum. *Colloids Surf. A: Physchem. Eng. Aspects*. 2002. **198-200**. P. 625–632. https://doi.org/10.1016/s0927-7757(01)00977-3.
34. Grytsenko K.P., Schrader S. Nanoclusters in polymer matrices prepared by co-deposition from a gas phase. *Adv. Colloid Interface Sci*. 2005. **116**. P. 263–276. https://doi.org/10.1016/j.cis.2005.04.005.
35. Grytsenko K., Lytvyn P., Slominski Y. Toward deposition of organic solid with controlled morphology on selected surfaces. *J. Appl. Phys. A*. 2019. **125**. P. 406–422. https://doi.org/10.1007/s00339-019-2699-1.
36. Grytsenko K., Ksianzou V., Kolomsarov Yu. *et al.* Fluoro-polymer film formation by electron activated vacuum deposition. *Surfaces*. 2021. **4**. P. 66–80. https://doi.org/10.3390/surfaces4010009.
37. Ksianzou V., Villringer C., Grytsenko K. *et al.* Structural and Optical Anomalies in Thin Films Grown in a Magnetic Field by Electron-Assisted Vacuum Deposition of PTFE. *Macromol. Mater. Eng.* 2025. **310**. 2400332. https://doi.org/10.1002/mame.202400332.
38. Price J.S., Wang B., Kim T. *et al.* Fluoropolymer-diluted small molecule organic semiconductors with extreme thermal stability. *Appl. Phys. Lett.* 2018. **113**. P. 263302. https://doi.org/10.1063/1.5053923.
39. Yudin S.G., Bodnarchuk V.V., Lazarev V.V. *et al.* Increasing of sensitivity and lifetime of organic photodiodes by doping with an inert polymer: A new photocurrent amplification mechanism. *Liq. Cryst. Appl.* 2019. **19**, No 4. 50–60. https://doi.org/10.18083/lcappl.2019.4.50.
40. Yokoyama D., Sasaki T., Suzuki Y. *et al.* Active refractive index control using a stably evaporable perfluororesin for high-outcoupling efficiency organic light-emitting diodes. *J. Mater. Chem. C.* 2021. **9**. P. 11115. https://doi.org/10.1039/d1tc02478g.
41. Kukla O.L., Grynko D.J., Pavluchenko A.S. *et al.* Chemoresistors based on nanocomposite gold-organic films. *Optoelectronics and Semiconductor Technique.* 2005. **40**. P. 127–135.

42. Lozovski V., Khihlovski S., Grytsenko K. *et al.* Modeling of optical absorption of three-component nanocomposite thin films. *phys. status solidi.* 2010. **249**. P. 2244–2251. https://doi.org/10.1002/pssb.200945154.
43. Kratochvíl J., Kuzminova A., Kylián O. State-of-the-art, and perspectives of silver/plasma polymer antibacterial nanocomposites. *Antibiotics.* 2018. **7**. P. 78. https://doi.org/10.3390/antibiotics7030078.
44. Caniglia G., Sportelli M.C., Heinzmann A. *et al.* Silver-fluoropolymer (Ag-CFX) films: Kinetic study of silver release, and spectroscopic-microscopic insight into the inhibition of *P. fluorescens* biofilm formation. *Anal. Chim. Acta.* 2022. **1212**. P. 339892. https://doi.org/10.1016/j.aca.2022.339892.
45. Bonilla-Gameros L., Chevallier P., Delvaux X. *et al.* Fluorocarbon plasma-polymerized layer increases the release time of silver ions and the antibacterial activity of silver-based coatings. *Nanomaterials.* 2024. **14**. P. 609. https://doi.org/10.3390/nano14070609.
46. Hartig T., Paulsen J., Drewes J. *et al.* Functional polymer nanocomposites by gas aggregation cluster source and initiated chemical vapor deposition, *Adv. Mater. Technol.* 2025. **10**, No 9. P. 2401763. https://doi.org/10.1002/admt.202570048.
47. He C., Rogachev A.V., Li B. *et al.* Synthesis and structure of antibacterial coatings formed by electron-beam dispersion of polyvinyl chloride in vacuum. *Surf. Coat. Technol.* 2018. **354**. P. 38–45. https://doi.org/10.1016/j.surfcoat.2018.09.013.
48. Nunes J., Piedade A.P. Nanoindentation of functionally graded hybrid polymer/metal thin films, *Appl. Surf. Sci*. 2013. **284**. P. 792–797. https://doi.org/10.1016/j.apsusc.2013.08.009.
49. Pinho A., Piedade A. Polymeric coatings with antimicrobial activity. *Polymers.* 2020. **12**. P. 2469. https://doi.org/10.3390/polym12112469.
50. Senda K., Matsuda T., Kawanishi T. *et al.* Preparation of a functionally graded fluoropolymer thin film and its application to antireflective coating. *Jpn. J. Appl. Phys.* 2013. **52**. P. 05DB01. https://doi.org/10.7567/jjap.52.05db01
51. Usui H. Physical vapor deposition of polymer thin films. *Jpn. J. Appl. Phys.* 2025. **64**. P. 030802. https://doi.org/10.35848/1347-4065/adb439.

Authors' contributions

Grytsenko K.P.: conceptualization, methodology, writing – original draft.
Kukla O.L.: project administration, validation.
Biletskiy A.I.: formal analysis, data curation, resources.
Kashyna H.S.: conceptualization, supervision.
Kutafin Y.V.: methodology, resources.
Prelipceanu M.: writing – original draft, visualization, resources.
Grebinyk A.: writing – original draft, resources.
Vashchilina E.V.: writing – review & editing.

Authors and CV

K.P. Grytsenko, PhD in Materials Science at the Kharkov Institute of Monocrystals, 2000. Since 1999 he is working at the V. Lashkaryov Institute of Semiconductor Physics, NAS of Ukraine, when he obtained scientific rank of Senior Research Scientist in 2004. Area of his scientific activity includes the development of both compounds and deposition technology for production of hybrid nanocomposite thin films for various optoelectronics applications, including optical memory, optical sensors and biotechnology.
https://orcid.org/0000-0002-2956-3654

O.L. Kukla received his PhD (2000) and Doctor of Sciences (2016) degrees in Physics of Devices, Elements and Systems at the V. Lashkaryov Institute of Semiconductor Physics. He is the Leading Scientist of the Department of Chemobiosensorics. The area of his scientific activity include the development and design of chemical and biological sensors and sensor arrays for biotechnology, medicine and ecology, study of molecular adsorption effects in polymer, biopolymer and composite thin layers.
E-mail: alex.le.kukla@gmail.com,
https://orcid.org/0000-0003-0261-982X

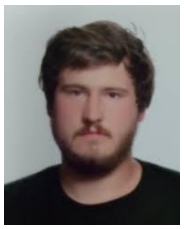

A.I. Biletskiy graduated from the Taras Shevchenko Kyiv National University in 2021 with M.S. in applied physics. Since 2023 he is the post-graduate student at the Institute of Semiconductor Physics, NAS of Ukraine, and since 2024 he works there as engineer. His professional activities include the development of optical measuring setup based on surface plasmon resonance, the study of spectroscopy of radiation from plasmon-photon scattering in thin films of high conducting materials.
E-mail: belanton11@gmail.com,
https://orcid.org/0009-0007-2074-3839

Hanna Kashyna received PhD in 2012 and Doctor of Sciences degree (2020) at the National Pedagogical University named after M.P. Drahomanov. She holds the academic title of Professor. She is the Head of the Department of Intelligent Systems and Digital Technologies at the Academy of Labor, Social Relations and Tourism. Her scientific activities include modeling of various nanomaterials.
E-mail: g.kashina@npu.edu.ua,
https://orcid.org/ 0000-0002-2829-9847

Yurii Kutafin, PhD in Electronics from the National Technical University of Ukraine "Igor Sikorsky Kyiv Polytechnic Institute", 2024. Since 2025 he works at the Academy of Labour, Social Relations and Tourism. His scientific activities include development of methods for modeling and optimizing the electrical characteristics of current circuits, as well as the design and development of image processing applications.
E-mail: yurkut@gmail.com,
https://orcid.org/0000-0002-8156-1277

Anna Grebinyk received Master of BioChemistry from the Taras Shevchenko University of Kyiv (2013) and PhD at the University of Wurzburg (2021). From 2015 to present she is the researcher of University of Applied Sciences, Wildau, Germany. Since 2022 she is also the Head of PITZ Biolab, Photo Injector Test Facility at German Electron Synchrotron (DESY). Areas of her research include: nanomaterials, nanoparticles-mediated drug delivery, photodynamic and X-ray therapy of cancer. https://orcid.org/0000-0002-4651-7908, e-mail: grebinyk.ann@gmail.com

Marius Prelipceanu, PhD in Electronics and Telecommunications from the "Stefan cel Mare" University of Suceava, Romania (2014) and M.S. in Organic Semiconductors Thin Films (2004) from "Al. I. Cuza" University of Iasi (Romania) and Potsdam University (Germany). The studies summarized as follows: the construction and investigation of optoelectronic devices, tailored with a new series of organic and hybrid nanocomposite materials, by means of electrical, optical and morphology characterization, as well as theoretical modeling. E-mail: marius.prelipceanu@usm.ro,
https://orcid.org/0000-0001-5831-721

Olena Vashchilina, PhD in Physical and Mathematical Sciences (2005). Since 2019 she is working as Associate Professor at the Department of Applied Information Systems, Faculty of Information Technology, Taras Shevchenko National University of Kyiv. The area of her scientific activity includes the application of information technologies to the study of complex systems, particularly in the fields of optoelectronics and thin film physics.
E-mail: olenavashchilina@knu.ua,
https://orcid.org/0000-0001-6867-6216

Тонкі композитні плівки з перфторполімерною матрицею, осаджені з газової фази: властивості та нові сфери застосування (Огляд)

К.П. Гриценко, О.Л. Кукла, А.І. Білецький, Г.С. Кашина, Ю.В. Кутафін, М. Преліпчану, А. Гребінник, Е.В. Ващіліна

Анотація. В огляді узагальнено властивості та сфери застосування нанокомпозитних тонких плівок на основі перфторполімерів, отриманих шляхом осадження з газової фази, та розглядаються тенденції розвитку цієї галузі. Перфторполімерна матриця захищає металеві наночастинки від корозії, надає поверхням супергідрофобні властивості, подовжує термін служби медичних імплантатів, покращує характеристики функціональних шарів в органічних світлодіодах тощо. Барвники та металеві наночастинки, вбудовані в перфторполімерні матриці, проявляють унікальні властивості, а органічні молекули, вбудовані в такі матриці, демонструють виняткову стабільність, що робить ці матеріали перспективними для застосування в оптиці та біомедицині.

Ключові слова: перфторполімер, політетрафторетилен, тонкі плівки, матриця, нанокомпозит, барвник.